Fuzheng Kang'ai decoction suppresses hepatocellular carcinoma via regulation of the KLF4/HIF-1α/CA9 signaling axis

Yi Cui[1], Yuhan Zhang[1], Jinwei Zhang[2], Zhenghong Chen[3], Bin Yuan[3], Wenjuan Chen[4], Le Han[5], Bin Zhao[6], Yili Zhang[4], Peixi Zhao[1, 7]

[1]Department of Pharmacy, Shaanxi Cancer Hospital, Xi'an, Shaanxi, China
[2]Health Science Center, Xi'an Jiaotong University, Xi'an, Shaanxi, China
[3]Department of Integrated Traditional Chinese and Western Medicine, Shaanxi Cancer Hospital, Xi'an, Shaanxi, China
[4]Third Department of Internal Medicine, Shaanxi Cancer Hospital, Xi'an, Shaanxi, China
[5]Department of Thoracic Surgery, Shaanxi Cancer Hospital, Xi'an, Shaanxi, China
[6]Department of Scientific Research and Education, Shaanxi Cancer Hospital, Xi'an, Shaanxi, China
[7]School of Life Science and Technology, Xi'an Jiaotong University, Xi'an, Shaanxi, China

Submitted: 7 November 2025; **Accepted:** 5 January 2026
Online publication: 1 April 2026

Arch Med Sci
DOI: https://doi.org/10.5114/aoms/216399

***Corresponding authors:**
*Corresponding authors:
Prof. Yili Zhang, PhD
Third Department
of Internal Medicine
Shaanxi Provincial
Cancer Hospital
No. 309 Yanta West Road
Xi'an 710061
Shaanxi, China
E-mail: doctor_z2023@stu.xjtu.edu.cn

Prof. Peixi Zhao, PhD
Department of Pharmacy
Shaanxi Provincial
Cancer Hospital
No. 309 Yanta West Road
Xi'an 710061
Shaanxi, China
E-mail: Dr_zhaopx@163.com

Abstract

Introduction: Clinical studies have established the efficacy of Fuzheng Kang'ai formula (FZKAF) in hepatocellular carcinoma (HCC) management. The molecular basis of FZKAF's HCC-suppressive effects is not fully characterized. This investigation aimed to mechanistically delineate FZKAF's therapeutic actions against HCC.

Material and methods: Phytochemical characterization via liquid chromatography-mass spectrometry (LC-MS) established the decoction's bioactive constituents. CCK-8 assays quantified proliferative suppression and cytotoxicity, while Annexin V-FITC/PI staining and cell cycle analysis mapped apoptosis induction. Integrated proteomic and transcriptomic profiling screened core targets and signaling pathways. Therapeutic efficacy was ultimately confirmed in an orthotopic HCC nude mouse model.

Results: Phytochemical profiling identified 33 bioactive compounds in serum following FZKAF administration, including 9 established anti-tumor agents such as paeoniflorin, catechin, kaempferol, and quercetin. Functionally, FZKAF demonstrated dual anti-HCC efficacy by suppressing tumor growth *in vivo* and inhibiting 97H cell proliferation in vitro while promoting apoptosis through mitochondrial dysfunction. Mechanistic interrogation via multi-omics revealed FZKAF coordinately modulates KLF4, HIF-1α, and CA9 targets to disrupt oncogenic signaling.

Conclusions: FZKAF orchestrates apoptosis induction and growth suppression in HCC, at least partially, by modulating the KLF4/HIF-1α/CA9 signaling axis, revealing a novel druggable pathway that advances precision oncology strategies for HCC patients.

Key words: hepatocellular carcinoma, Fuzheng Kang'ai decoction, traditional Chinese medicine, phytochemicals, bioactive components.

Introduction

Based on the latest cancer statistics report, the global incidence of liver cancer reached 865,269 new cases with 757,948 deaths, ranking as

the sixth most prevalent cancer worldwide [1]. In China, liver cancer accounted for 367,700 newly diagnosed cases and 316,500 deaths, indicating that Chinese patients represent 42.5% of the global liver cancer burden [2]. Hepatocellular carcinoma (HCC), a highly lethal primary liver cancer, accounts for 90% of all primary liver malignancies [3, 4]. It predominantly occurs in patients with viral hepatitis infections and exhibits a 5-year survival rate below 20% [3, 4]. HCC progresses insidiously with high malignancy and early distant metastasis [3, 4]. Consequently, most patients are diagnosed at stages precluding surgical intervention [3, 4]. Furthermore, targeted therapies and immunotherapies often induce treatment resistance and clinically significant toxicities [5]. While surgical resection and pharmacotherapy remain the clinical mainstays, traditional Chinese medicine (TCM) has demonstrated distinctive efficacy in HCC management combined with surgery, chemotherapy, targeted therapy, and immunotherapy [5, 6]. It not only alleviates cancer-related symptoms but also significantly improves patients' quality of life and prolongs overall survival [7–10]. Therefore, in-depth investigation of HCC from TCM perspectives carries substantial clinical value, serving as a critical complementary therapeutic approach in contemporary HCC management.

Current evidence reveals that numerous TCM monomers and compound formulations, including Biejia-Ruangan, Fuzheng Huayu, Fuzheng Jiedu Xiaoji formulation, sinomenine, and paeoniflorin, have demonstrated significant anti-HCC activity in both preclinical and clinical studies [8, 11–14]. Fuzheng Kang'ai decoction (FZKAF), a standardized TCM formulation clinically applied in China for over two decades, has been primarily investigated in non-small cell lung cancer (NSCLC) across preclinical and clinical studies [15, 16]. FZKAF potentiates gefitinib's antitumor efficacy by enhancing drug sensitivity in lung cancer models [17, 18]. Additionally, it exerts antineoplastic effects through modulation of multiple signaling pathways including ferroptosis regulation, epidermal growth factor receptor (EGFR) signaling transduction, DNA methyltransferase 1 (DNMT1) activity, and phosphatase and tensin homolog deleted on chromosome 10 (PTEN)-mediated tumor suppression [15, 19–22]. Notably, research on FZKAF's efficacy against HCC remains limited. This study will critically examine FZKAF's antitumor activity in HCC and elucidate its underlying molecular mechanisms.

It is well established that TCM compound formulations target multiple molecular pathways against HCC [9, 23, 24]. A systematic review and meta-analysis identified 247 herb-targeted genes and 36 core therapeutic genes. Pathway enrichment analysis revealed significant involvement of the hypoxia-inducible factor 1 (HIF-1) signaling pathway and programmed death-ligand 1 (PD-L1) immune checkpoint axis in HCC pathogenesis [9]. To further elucidate potential therapeutic targets of FZKAF in HCC, we employed integrated transcriptomics and proteomics analyses, identifying Kruppel-like factor 4 and hypoxia-inducible factor-1α (KLF4/HIF-1α) as candidate targets. Subsequent validation was performed using complementary *in vitro* models and in vivo mouse xenograft experiments to confirm FZKAF's antitumor efficacy against HCC.

Material and methods

FZKAF formula

The FZKAF formula is an empirically modified prescription derived from the classical formulas Si-Jun-Zi-Tang and Chaihu-Shugan-San through syndrome differentiation. Clinically indicated for mid-to-late stage HCC patients presenting with liver depression-spleen deficiency syndrome and congealed toxin accumulation, its composition includes: *Codonopsis Radix* (Dang Shen; 30 g), stir-fried *Atractylodis Macrocephalae Rhizoma* (Chao Bai Zhu; 30 g), stir-fried *Dioscoreae Rhizoma* (Chao Shan Yao; 30 g), *Scutellariae Barbatae Herba* (Ban Zhi Lian; 30 g), *Hedyotis Diffusa Herba* (Bai Hua She She Cao; 30 g), *Trionycis Carapax* (Bie Jia; 30 g), *Astragali Radix* (Huang Qi; 45 g), *Poria* (Fu Ling; 15 g), *Curcumae Rhizoma* (E Zhu; 15 g), *Bupleuri Radix* (Chai Hu; 15 g), *Ganoderma* (Ling Zhi; 15 g), *Crataegi Fructus* (Sheng Shan Zha; 15 g), *Curcumae Longae Rhizoma* (Jiang Huang; 10 g), *Glycyrrhizae Radix et Rhizoma* (Gan Cao; 6 g); *Citri Reticulatae Pericarpium* (Chen Pi; 12 g), *Curcumae Radix* (Yu Jin; 12 g), *Paeoniae Radix Alba* (Bai Shao; 12 g), and *Scolopendra* (Wu Gong; 3 g) as described previously [17]. According to the calculation based on the above herbal formula, the daily human dose is 355 g of FZKAF.

Reagents

The following reagents were employed in the study: DMEM (C11995500BT, Gibco); fetal bovine serum (AC101, Gibco); CCK-8 kit (Beyotime Biotechnology Co., Ltd.); Annexin V-FITC/PI apoptosis detection kit (559763, BD Biosciences, USA); cell cycle detection kit (AC101, Vazyme Biotech Co., Ltd.); recombinant anti-KLF4 antibody (ab215036, Abcam); anti-HIF-1α antibody (ab51608, Abcam, UK); anti-Carbonic Anhydrase 9 (CA9) antibody (ab108351, Abcam, UK); BAX antibody (GB15690, Servicebio, China); Bcl-2 antibody (GB154380, Servicebio, China); GAPDH (GB15004, Servicebio); HRP-goat anti-rabbit secondary antibody (GB23303, Servicebio, China).

Extraction of FZKAF and preparation of medicated serum. All herbs in the FZKAF were pre-

pared according to the traditional decoction method. All herbs were soaked in distilled water for 30 min, heated to 100°C, decocted twice, and then filtered through gauze and concentrated. The concentrated solution was kept at 4°C before combining.

Thirty healthy adult Sprague-Dawley (SD) rats (body weight: 150–170 g) were randomly divided into a control group (n = 15) and FZKAF group (n = 15) and were purchased from the Experimental Animal Center of Xi'an Jiaotong University. Based on pharmacological experimental methods, the body surface area-based equivalent dose ratio between humans (70 kg) and rats (0.2 kg) is 0.018. The human dose of 355 g/70 kg was converted to a rat dose as follows: 355 g × 0.018 ÷ 0.2 kg = 31.95 g/kg. Rats in the FZKAF group received FZKAF via oral gavage at a dose of 31.95 g/kg. The control group received physiological saline, while the FZKAF group received the FZKAF decoction by an intragastric administration at a dose of 31.95 g/kg. Dosing was performed twice daily at 12-hour intervals for seven consecutive days. Before the final administration, the animals were fasted for 12 h with no access to water. One hour after dosing, anesthesia was induced and blood was collected from the aorta. The blood was kept at 4°C for 3 h, then centrifuged at 3,000 g for 15 min to obtain the pale yellow serum, which was heat-inactivated at 56°C for 30 min and filtered through a 0.22 µm membrane [25, 26]. The rats were housed (temperature: 22 ±2°C; humidity: 50 ±5%) at a constant temperature of 25 ±1°C with ad libitum access to food and water, in accordance with the requirements of the Animal Research: Reporting of In Vivo Experiments guidelines (version 2.0) [27].

Detection of FZKAF constituents absorbed into the bloodstream

Samples were divided into a blank serum group, an FZKAF-containing serum group, and an FZKAF extract solution group. For each group, 50 µg were taken, to which 400 µl of methanol was added, vortexed for 10 min, centrifuged at 13,000 rpm for 10 min, and the supernatant was collected for instrumental analysis. The chemical constituents of FZKAF were identified using a Q-Orbitrap high-resolution LC–MS instrument. High-resolution LC–MS data were matched and processed using Compound Discoverer 3.3 software and the mzCloud database to achieve qualitative analysis of the chemical components in FZKAF samples. The instrument used an electrospray ionization source with polarity-switching scans between positive and negative modes, a full mass/dd-MS2 acquisition mode, and a capillary temperature of 300°C. Sheath gas: nitrogen, 40 Arb; auxiliary gas: nitrogen, 15 Arb; spray voltage: 3.2 kV; data acquisition time: 30 min. Chromatographic conditions: column Waters HSS T3 (100 × 2.1 mm, 1.8 µm); mobile phases: A = ultrapure water with 0.1% formic acid, B = acetonitrile–isopropanol mixed solution with 0.1% formic acid; flow rate 0.3 ml/min; column temperature 40°C; injection volume 2 µl; gradient: 0 min A : B (90 : 10, v/v), 2 min A : B (90 : 10, v/v), 6 min A : B (40 : 60, v/v), 15 min A : B (40 : 60, v/v), 15.1 min A : B (90 : 10, v/v), 17 min A : B (90 : 10, v/v).

Cell culture

The human HCC cell line 97H was obtained from Starfish Biotech Co., Ltd. (Shanghai, China). The 97H cells were cultured in DMEM medium supplemented with 10% fetal bovine serum and incubated in a 37°C incubator with 5% CO_2.

Cell Counting Kit-8 (CCK-8)

97H cells in the logarithmic growth phase were trypsinized to obtain a single-cell suspension. The cells were seeded into 96-well plates at a density of 7 × 10^3 cells per well. Each well received FZKAF-containing serum at concentrations of 0, 2.5, 5, 10, 15, and 20%. After 48 h of incubation, the original medium was discarded. To each well, 100 µl of blank medium containing 10 µl of CCK-8 solution was added and incubated for an additional 1 h. Absorbance was measured at 450 nm using a microplate reader (OD value).

Flow cytometry and cell cycle distribution

Apoptosis of 97H cells induced by FZKAF-containing serum was assessed using an Annexin V-FITC/PI apoptosis detection kit. The cells were plated in a 6-well plate at a density of 5 × 10^5 cells per well and treated with FZKAF-L (7.5%) and FZKAF-H (15%)-containing serum for 48 h. After treatment, cells were collected and stained with the Annexin V-FITC/PI apoptosis detection kit, and the apoptosis rate was analyzed by flow cytometry. For cell cycle distribution analysis, cells were stained with 0.5 mg/ml propidium iodide (PI; Sigma-Aldrich; Merck KGaA) for 30 min, washed twice with PBS, resuspended in 500 µl of PBS, and analyzed by flow cytometry.

Transmission electron microscopy

Cells were seeded into a 6-well plate at 5 × 10^5 cells per well, divided into a blank group, FZKAF-L group (10% drug-containing serum), and FZKAF-H group (20% drug-containing serum), and treated for 48 h. The cell pellets were collected by centrifugation, resuspended in electron microscopy fixative at 4°C and fixed for 2–4 h, then stored at 4°C in fixative. Ultrastructure was observed us-

ing a transmission electron microscope (HT7800/HT7700, Hitachi, Japan).

Western blotting

97H cells were plated in six-well plates and treated with FZKAF-L and FZKAF-H drug-containing serum. After 48 h, cells were collected and lysed in a RIPA buffer containing PMSF and protease inhibitors. Protein concentration was determined by a BCA assay. Proteins were separated by 10% SDS-PAGE and transferred to PVDF membranes. Membranes were blocked with 5% non-fat milk and incubated with primary antibodies overnight at 4°C and HRP-goat anti-rabbit secondary antibody (dilution: 1 : 10,000) at 37°C for 1 h. Membranes were washed with PBST and detected by chemiluminescence, with imaging performed using a gel imaging system. Results were analyzed using ImageJ. Expression of apoptosis-related proteins Bax (dilution: 1 : 1000) and Bcl-2 (dilution: 1 : 1000), as well as signaling pathway proteins including KLF4 (dilution: 1 : 1000), HIF-1α (dilution: 1 : 1000), and CA9 (dilution: 1 : 1000), was assessed.

Establishment of a mouse orthotopic liver cancer model

Based on pharmacological experimental methods, the body surface area-based equivalent dose ratio between humans (70 kg) and nude mice (0.02 kg) is 0.0026. The human dose of 355 g/70 kg was converted to a murine dose as follows: 355 g × 0.0026 ÷ 0.02 kg = 46.15 g/kg. According to pharmacodynamic principles, animal studies typically establish low-, medium-, and high-dose groups in a 1 : 2 : 4 geometric progression. However, preliminary literature review indicates that common doses for nude mice are 31 g/kg and 59 g/kg [20, 22]. Therefore, this study adopted a 1 : 2 ratio with two dose groups: the low-dose group (46.15 g/kg) and high-dose group (92.30) g/kg (2× low dose) Notably, the 4× dose group was excluded due to administration volume constraints of oral gavage in nude mice. 97H-luc cells were cultured in the appropriate medium containing 10% fetal bovine serum. Exponentially growing cells were collected, resuspended in serum-free medium to a density of 5×10^7 cells/ml, and used for inoculation. Under isoflurane anesthesia of 16 mice (body weight: 20 ±2 g), an incision of about 1 cm was made along the ventral midline to expose the left liver lobe. The liver lobe was gently fixed with a PBS-soaked cotton swab. A 75 µl cell suspension was drawn into an insulin syringe, the liver capsule was punctured, and the cells were slowly injected under it. After injection, the needle was slowly withdrawn and the needle entry point pressed with a cotton swab to stop the bleeding. After hemostasis, the liver was gently pushed back into the abdomen, and the abdomen was closed layer by layer. The mouse was placed back in the cage and monitored regularly. Abdominal examinations were performed to determine whether tumor cells had engrafted and grown in the liver. One week after inoculation, *in vivo* imaging was performed, showing that all 16 mice had a clear fluorescence signal in the liver region. Based on the fluorescence signal strength in the liver region, mice were divided into four groups: blank control, model, FZKAF-L, and FZKAF-H. In the low-dose FZKAF group, 46.15 g/kg of FZKAF solution was administered by intragastric administration at 0.1 ml per mouse per dose; in the high-dose FZKAF group, 92.30 g/kg was administered by intragastric administration at 0.2 ml per mouse per dose. The model group received 0.2 ml of saline per mouse per dose by intragastric administration; the blank group received no treatment. Treatments were administered twice daily for 4 weeks. Tumor growth was monitored by small-animal *in vivo* imaging, mouse body weight was recorded, and the tumor growth inhibition rate was calculated. At the end of treatment, blood was collected from the abdominal aorta for assessment of biochemical indices.

Transcriptomics sequencing and data analysis

After the blank group and the FZKAF group (FZKAF-containing serum, 12.5%), with three biological replicates per group, underwent drug exposure for 48 h, Trizol was added to extract RNA (1 ml of Trizol per 5×10^6 cells). The lysate was transferred to a 2 ml tube, snap-frozen in liquid nitrogen for 0.5 h, and then stored at –80°C. Transcriptome sequencing was performed with assistance from Shanghai Applied Protein Technology Co., Ltd. The FeatureCounts tool was used to quantify expression levels of each gene in each sample, and results were reported in FPKM. Principal component analysis (PCA) plots and heatmaps were generated to visualize sample repeatability and differences. Differential expression analysis was performed with DESeq2, with *p*-values adjusted for multiple testing. Differentially expressed genes (DEGs) were identified using the criteria of adjusted p-value < 0.05 and $|\log_2$ fold change$| \geq 1$. DEGs were compared against all genes of the reference species based on Gene Ontology (GO) functional annotations. KEGG pathway enrichment analysis for the DEGs was conducted using KEGG pathway information, with the reference genome as background, and statistical significance was calculated by Fisher's exact test.

Proteomics analysis

Blank group and the FZKAF group (FZKAF-containing serum, 12.5%) were prepared with three

biological replicates and a drug exposure time of 48 h. The cells were washed twice gently by rocking in PBS cooled to 4°C, leaving a small amount of PBS in the dish, and then placed on ice. Cells were collected and stored at –80°C. Proteomics analysis was performed with assistance from Shanghai Applied Protein Technology Co., Ltd. Intergroup fold-changes in protein expression and *p*-values obtained from *t*-tests were used as evaluation criteria, and volcano plots were generated to visualize the statistical significance of intergroup protein differences. Hierarchical clustering was applied to classify differentially expressed proteins (DEPs), and the grouping results were visualized with a heatmap. GO and KEGG analyses were performed in a manner consistent with the transcriptomic analysis..

Statistical analysis

Data were expressed as mean and standard deviation. Statistical analysis was performed with the GraphPad Prism 9.0 (GraphPad Software, Inc., La Jolla, CA, USA). Parametric analyses were conducted after confirming that the data satisfied normality (Shapiro-Wilk, $\alpha = 0.05$) and variance homogeneity (Levene) criteria. Two-group comparisons followed a hierarchical approach: Normally distributed data with equal variances underwent Student's *t*-tests. When variance homogeneity was violated despite normality, Welch's corrected *t*-tests were implemented. Continuous variables failing normality assumptions were analyzed using the nonparametric Wilcoxon rank sum test (Mann-Whitney U test). For comparisons among three groups or more meeting parametric assumptions (normality and homogeneity of variance), one-way ANOVA was employed. When significant intergroup differences were detected ($p < 0.05$), post hoc pairwise comparisons were conducted using Tukey's honestly significant difference (HSD) test. Variance heterogeneity triggered Welch-ANOVA implementation. Non-normal distributions were analyzed via Kruskal-Wallis tests with Dunn-Bonferroni corrected pairwise comparisons. A *p*-value of less than 0.05 was considered to indicate a significant difference.

Results

Detection of FZKAF constituents. FZKAF was analyzed separately in positive and negative ion modes. Through integration of the total ion current chromatogram (Figures 1 A, B), MS/MS spectral data, and relevant literature, 32 major compounds in FZKAF were tentatively identified (Table I). Subsequent screening using the TCMSP database with thresholds of oral bioavailability (OB) ≥ 30% and drug-likeness (DL) ≥ 0.18 combined with literature-reported compounds demonstrating systemic absorption and well-established pharmacological activity yielded nine potential bioactive components of FZKAF: albiflorin, eicosadienoic acid, catechin, coumarin, kaempferol, quercetin, arachidonic acid, equilin, and ergosterol peroxide.

Transcriptome sequencing analysis

Cluster heatmaps were generated using gene expression data across samples to visualize expression variations and clustering relationships. The analysis revealed distinct segregation between the FZKAF and control groups in terms of gene expression patterns and correlative relationships within the clustered heatmap (Figure 2 A). Differential expression analysis using DESeq2 identified 205 DEGs between FZKAF-treated and control groups, comprising 42 upregulated and 163 downregulated genes (Figure 2 B). Subsequent KEGG and GO enrichment analyses were performed using the DEGs. The results visualized the top 20 enriched KEGG pathways (Figure 2 C) along with the top 10 significantly enriched terms in each GO category (Figure 2 D): molecular functions (MF), cellular components (CC), and biological processes (BP). Through transcriptomic analysis of significantly differentially expressed genes, key genes within the HIF-1 signaling pathway exhibited marked downregulation: VEGFA (log_2FC: 0.243), TXNIP (log_2FC: –1.75), CA9 (log_2FC: –2.45), NDUFA4L2 (log_2FC: –2.30),

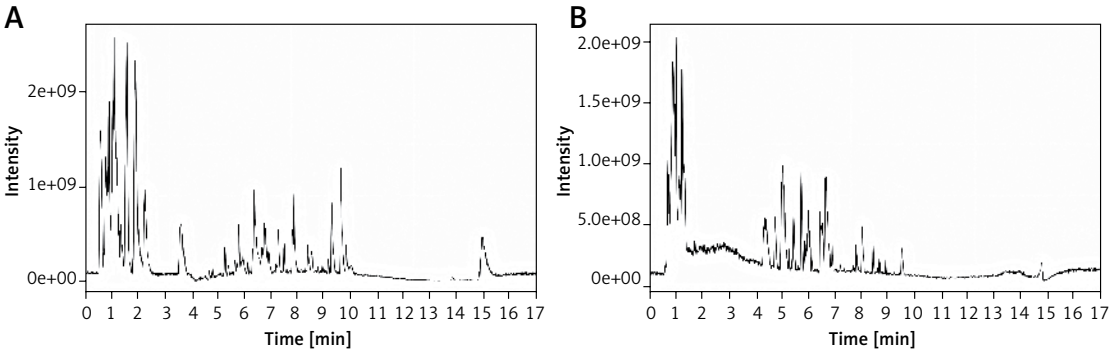

Figure 1. Base peak chromatograms of FZKAF. (**A**) BPC in positive ion mode; (**B**) BPC in negative ion mode

Table I. Chemical composition identification information of FZKAF

Metabolite 2	Retention time [min]	Mode	Adducts	Formula	m/z	Fragmentation Score	FZKAF2
Ganoderic acid C6	7.637	Neg	M-H	C30H42O8	529.281	95.600	2315.073
18 β-Glycyrrhetinic acid	12.308	Neg	M-H	C30H46O4	469.333	86.300	724379.112
Sucrose	0.783	Neg	M-H, M + FA-H, 2M-H	C12H22O11	341.110	83.000	15836989.450
Mirificin	4.934	Neg	M-H, M + FA-H	C26H28O13	593.154	82.500	5969.581
Rubrofusarin	9.950	Neg	M-H2O-H	C15H12O5	253.051	76.500	1120790.832
Apigenin 7-O-methyl-glucuronide	5.801	Neg	M + K-2H	C21H34O14	547.146	73.100	543951.867
Rehmannioside C	5.801	Neg	M + K-2H	C21H34O14	547.146	73.100	543951.867
Methyl gallate	4.276	Neg	M-H	C8H8O5	183.030	70.700	80585.311
Hesperetin	7.841	Neg	M-H	C16H14O6	301.072	68.100	3406495.091
Cedrusin	7.739	Neg	M + FA-H	C19H22O6	391.141	63.300	634782.226
Scutellarin methyl ester	6.479	Neg	M-H, 2M-H	C22H20O12	475.089	62.200	10903086.770
Euphroside	1.037	Neg	M + Cl	C16H24O10	411.107	62.100	442011.278
Alizarin	8.859	Neg	M-H	C14H8O4	239.035	60.800	81640.917
Purpurin	7.278	Neg	M + FA-H	C14H8O5	301.036	59.700	4226594.716
13-Deoxy-isogibberellic acid	7.368	Neg	M + FA-H	C19H22O5	375.146	59.600	889475.227
Monodictyxanthone	8.746	Neg	M-H2O-H	C15H10O5	251.035	58.500	2225980.759
Eupalinilide B	8.234	Neg	M-H	C20H24O6	359.151	58.400	460205.645
Pinobanksin	6.903	Neg	M + FA-H	C17H14O6	359.078	61.700	251339.587
Oleuroside	5.291	Neg	M-H, M + K-2H	C25H32O13	539.177	52.300	20756615.760
Oroxylin A-7-O-β-D-glucuronide	7.258	Pos	M + H	C22H20O11	461.107	98.200	1417255.471
Wogonoside	7.522	Pos	M + H	C22H20O11	461.107	97.500	4415670.531
14-Benzoylaconine	6.206	Pos	M + H	C32H45NO10	604.311	93.500	903288.274
Saikosaponin B1	8.644	Pos	M + H-H2O, M + Na, M + H, M + K, M + H-2H2O	C42H68O13	763.462	93.300	3411793.088
Isomeranzin	8.917	Pos	M + H	C15H16O4	261.112	91.400	129386.868
Naringenin chalcone	5.036	Pos	M + H	C15H12O5	273.076	87.600	232803.943
Allocryptopine	5.839	Pos	M + H	C21H23NO5	370.165	71.800	280676.398
Pectolinarigenin	9.479	Pos	M + H	C17H14O6	315.086	71.000	653531.181
Desoxo-narchinol A	9.823	Pos	M + H-H2O	C12H16O2	175.112	65.900	340367.092
Altamisic acid	7.810	Pos	M + H-2H2O	C15H20O5	245.117	64.700	101039.346
Pterosin G	5.913	Pos	M + CH3OH + H	C14H18O3	267.159	56.200	723765.126
Scutebata F	9.926	Pos	M + H	C30H37NO9	556.254	52.300	2805814.014
Chasmanine	5.203	Pos	M + H, M + Na	C25H41NO6	452.300	52.100	128445.430

and EGR1 (log_2FC: –0.10). These genes are functionally implicated in tumor angiogenesis and energy metabolism, suggesting that FZKAF may disrupt tumor hypoxic adaptation by suppressing the HIF-1 pathway. Concurrently, pivotal genes in the epithelial-mesenchymal transition (EMT) pathway were significantly inhibited: LAMC2 (log_2FC: 1.49), VIL1 (log_2FC: –1.40), CLDN7 (log_2FC: –1.12), and TGFBI (log_2FC: –0.52).

Proteomics analysis

DEPs were screened using thresholds of |FC| > 1.2 and $p < 0.05$. Visualization through cluster heatmap (Figure 3 A) and volcano plot (Figure 3 B) revealed 391 DEPs between FZKAF-treated and control groups, comprising 263 upregulated and 128 downregulated proteins. Subsequent KEGG and GO enrichment analyses were performed using these DEPs, with the results illustrating the top 20 enriched KEGG pathways (Figure 3 C) alongside significantly enriched terms across GO categories (Figure 3 D), including MF, CC, and BP. Quantitative proteomic analysis revealed significant alterations in key proteins associated with the HIF-1α signaling pathway (KLF4: 1.5-fold; CA9: 0.184-fold) and ferroptosis regulators: GPX3: 2.51-fold ($p < 0.001$),

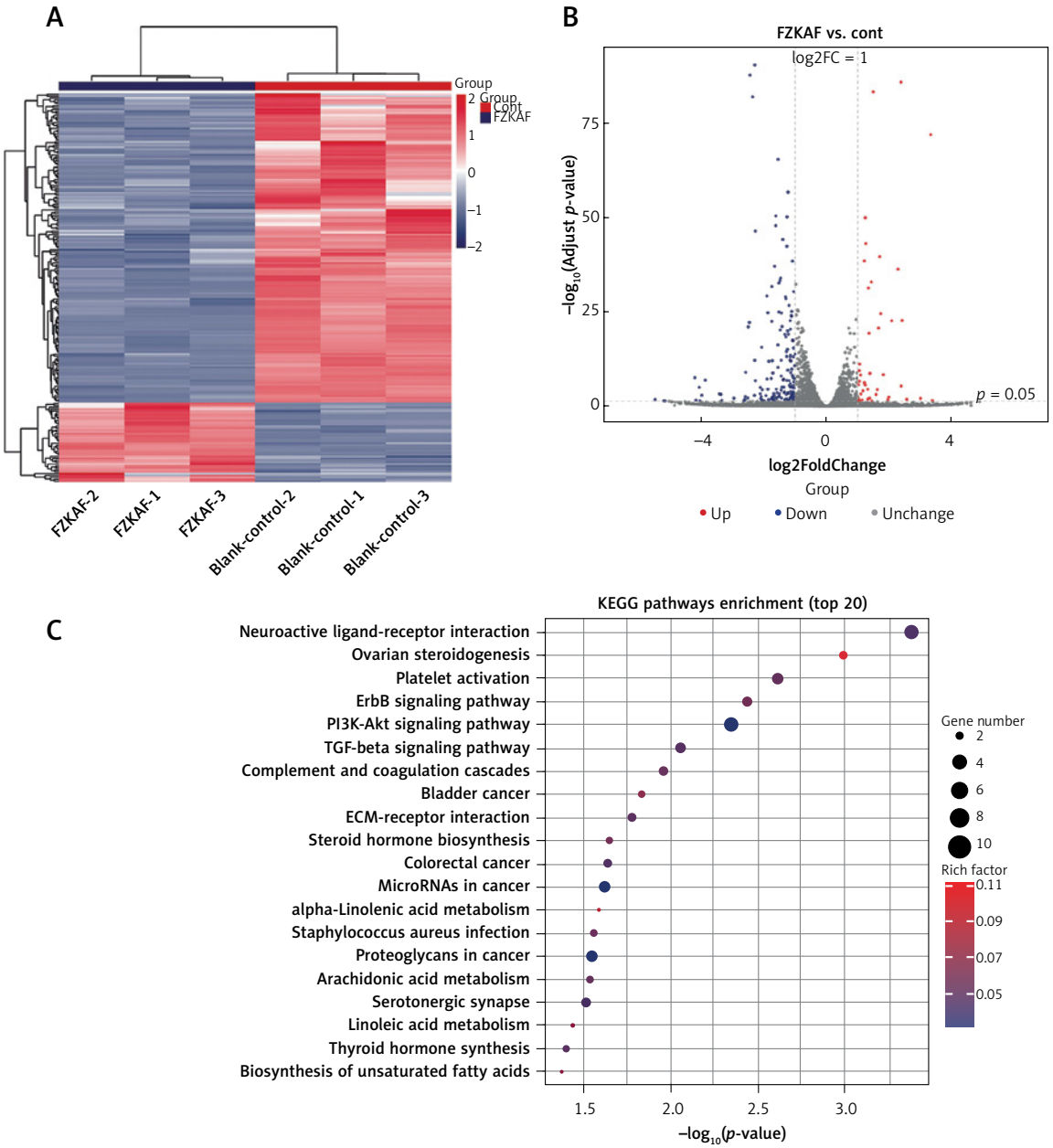

Figure 2. Transcriptome sequencing analysis. After treating the vehicle control group and FZKAF group (12.5% v/v FZKAF-containing serum), total RNA was extracted from 97H cells for RNA sequencing analysis. **A** – Hierarchical clustering of DEGs. **B** – Volcano plot of DEGs. **C** – KEGG enrichment analysis

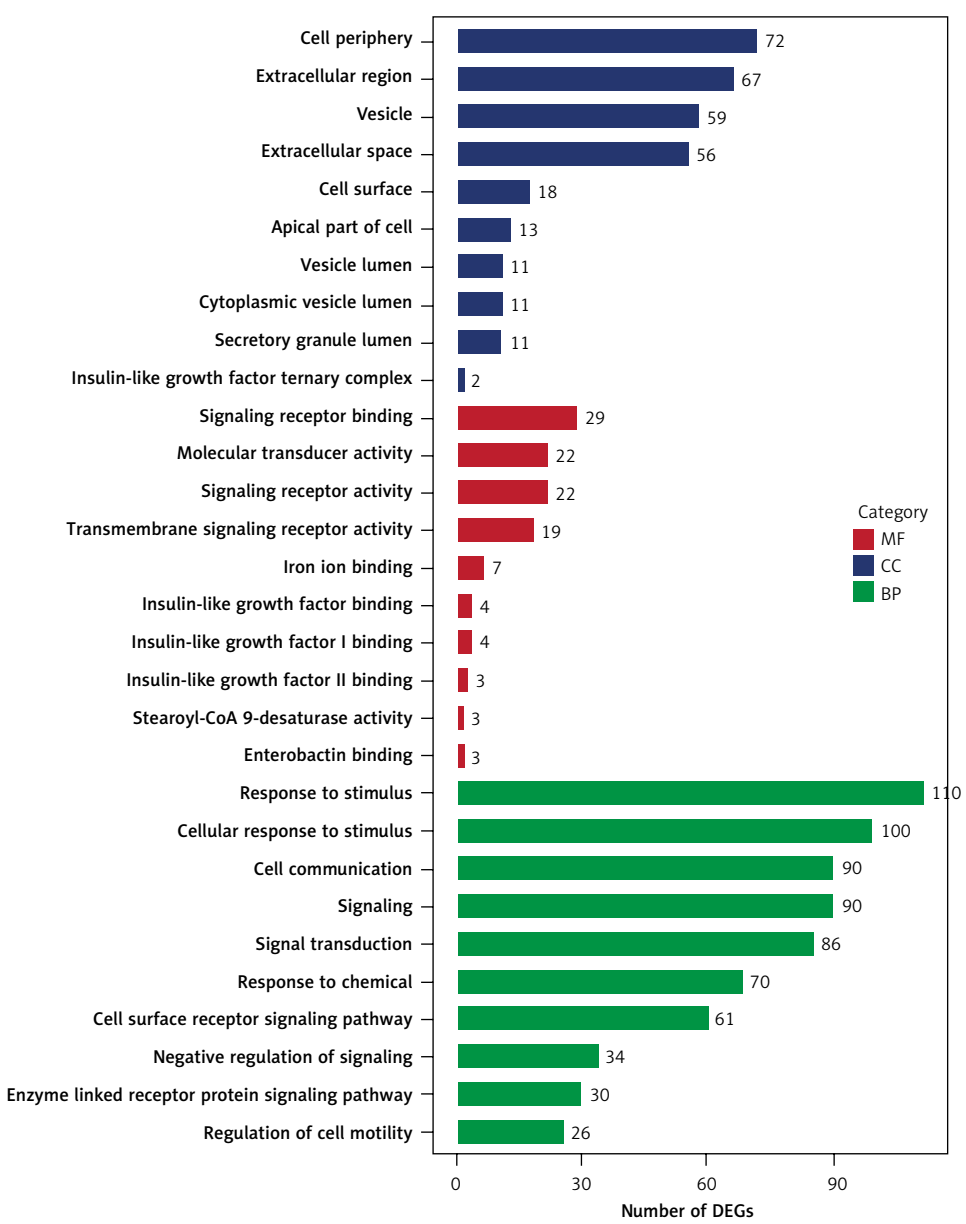

Figure 2. Cont. **D** – GO functional annotation analysis

FTH1: 2.90-fold ($p < 0.001$), FTL (ferritin light chain): 3.35-fold ($p < 0.001$), PLIN2 (lipid droplet protector): 2.09-fold ($p < 0.001$). These findings suggest that FZKAF may induce iron-dependent lipid peroxidation by suppressing GPX3 activity and/or depleting glutathione reserves.

Orthotopic HCC models in nude mice and anti-tumor activity of FZKAF

In vivo imaging revealed focal purple fluorescence in the liver region immediately after implantation (Figure 4 A). By one week after implantation (Figure 4 B), the signal intensity had substantially increased and diffused to cover > 60% of the hepatic area, confirming successful tumor engraftment.

As demonstrated in Figure 5 A and Table II, FZKAF-H significantly reduced liver tumor weight ($p < 0.01$) by 34.5% compared to the model group. Concurrently, FZKAF exerted hepatoprotective effects (Figure 5 B), as evidenced by significantly lowered serum ALT and AST levels across all treatment groups versus the model group, indicating mitigation of HCC-associated liver injury. Furthermore, FZKAF improved survival outcomes in tumor-bearing mice (Table III): during post-administration days 0–7, treated animals maintained superior food intake and mental alertness. By day 7, model group mice developed cachectic manifestations, including reduced mobility and fecal output, due to rapid tumor progression, whereas FZKAF groups exhibited more stable weight gain.

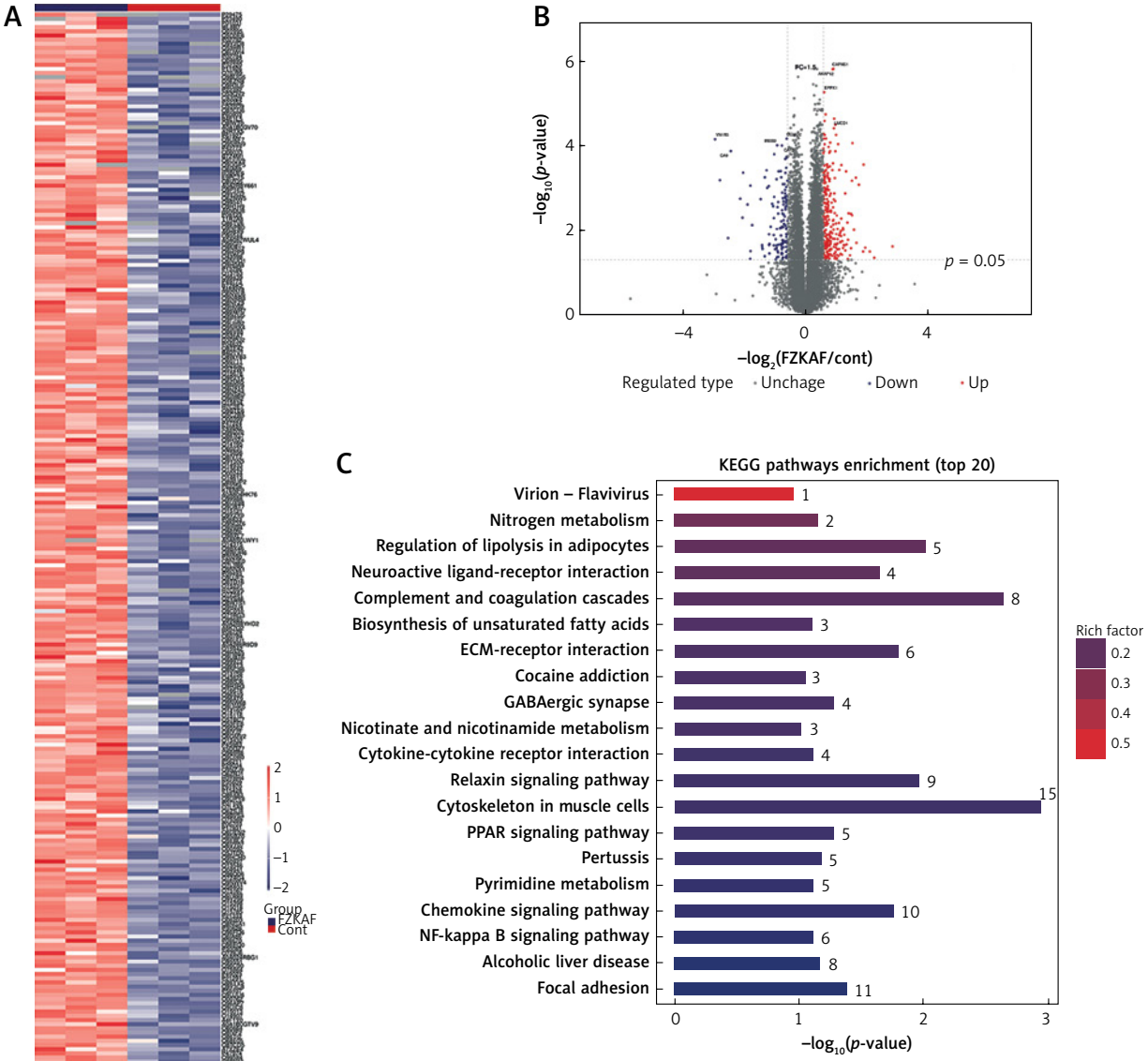

Figure 3. Proteomics analysis. After treating the vehicle control group and FZ-KAF group (12.5% v/v FZKAF-containing serum), total protein was extracted from 97H cells. **A** – Hierarchical clustering of DEPs. **B** – Volcano plot of DEPs. **C** – KEGG enrichment analysis

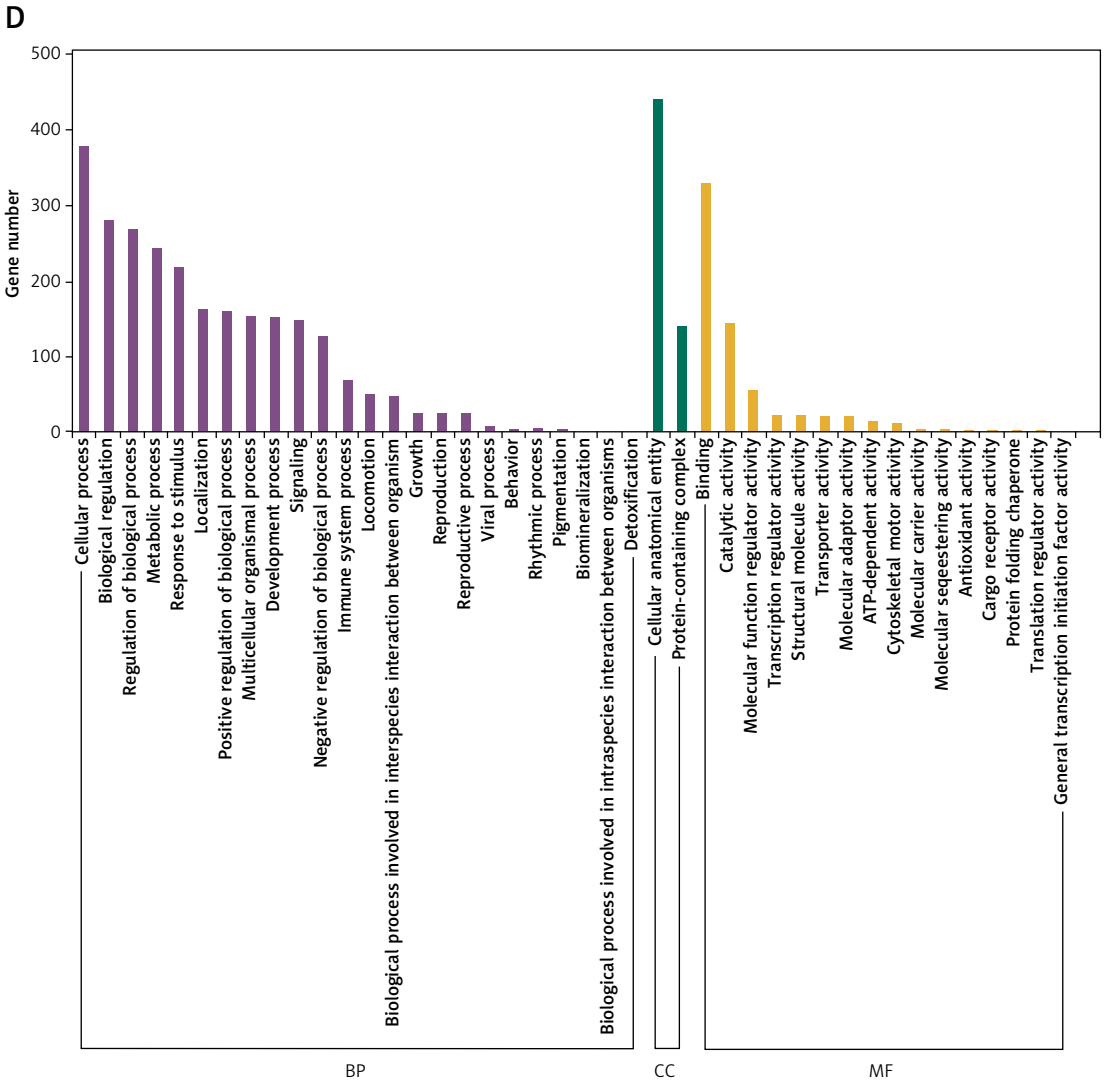

Figure 3. Cont. **D** – GO functional annotation analysis

Critically, the high-dose group maintained significantly higher body weight than the model group by day 25 ($p < 0.05$), demonstrating effective alleviation of cancer-associated wasting syndrome.

FZKAF inhibits 97H cell proliferation

CCK-8 assay results demonstrated that FZKAF significantly inhibited the proliferation of 97H cells in a dose-dependent manner. After 48 h of treatment, the IC_{50} value for FZKAF was determined to be 12.5% v/v drug-containing serum. Cell proliferation inhibition rates progressively increased with escalating concentrations of FZKAF-containing serum (Figure 6).

FZKAF induces 97H cell apoptosis and cell cycle arrest

Annexin V-FITC/PI apoptosis assay confirmed that FZKAF induced apoptosis in 97H cells. Compared to the control group, the FZKAF-H group exhibited a significant increase in apoptotic cells (control: 8.39 ±1.25% vs. FZKAF-H: 15.18 ±1.21%; Figure 7 A). Concurrent cell cycle analysis revealed that both FZKAF-H and FZKAF-L groups showed a marked increase in the proportion of cells in S-phase, indicating FZKAF-induced S-phase cell cycle arrest (Figure 7 B).

Effects of FZKAF on cell morphology

TEM analysis revealed distinct morphological alterations among the three treatment groups following exposure to control serum and FZKAF-containing serum. In the control group (Figure 8 A), cells exhibited moderate ultrastructural damage characterized by mildly dilated perinuclear spaces, partially pyknotic mitochondria, and slightly expanded rough endoplasmic reticulum (RER). The FZKAF-L group (Figure 8 B) demonstrated comparatively less severe changes: perinuclear spaces re-

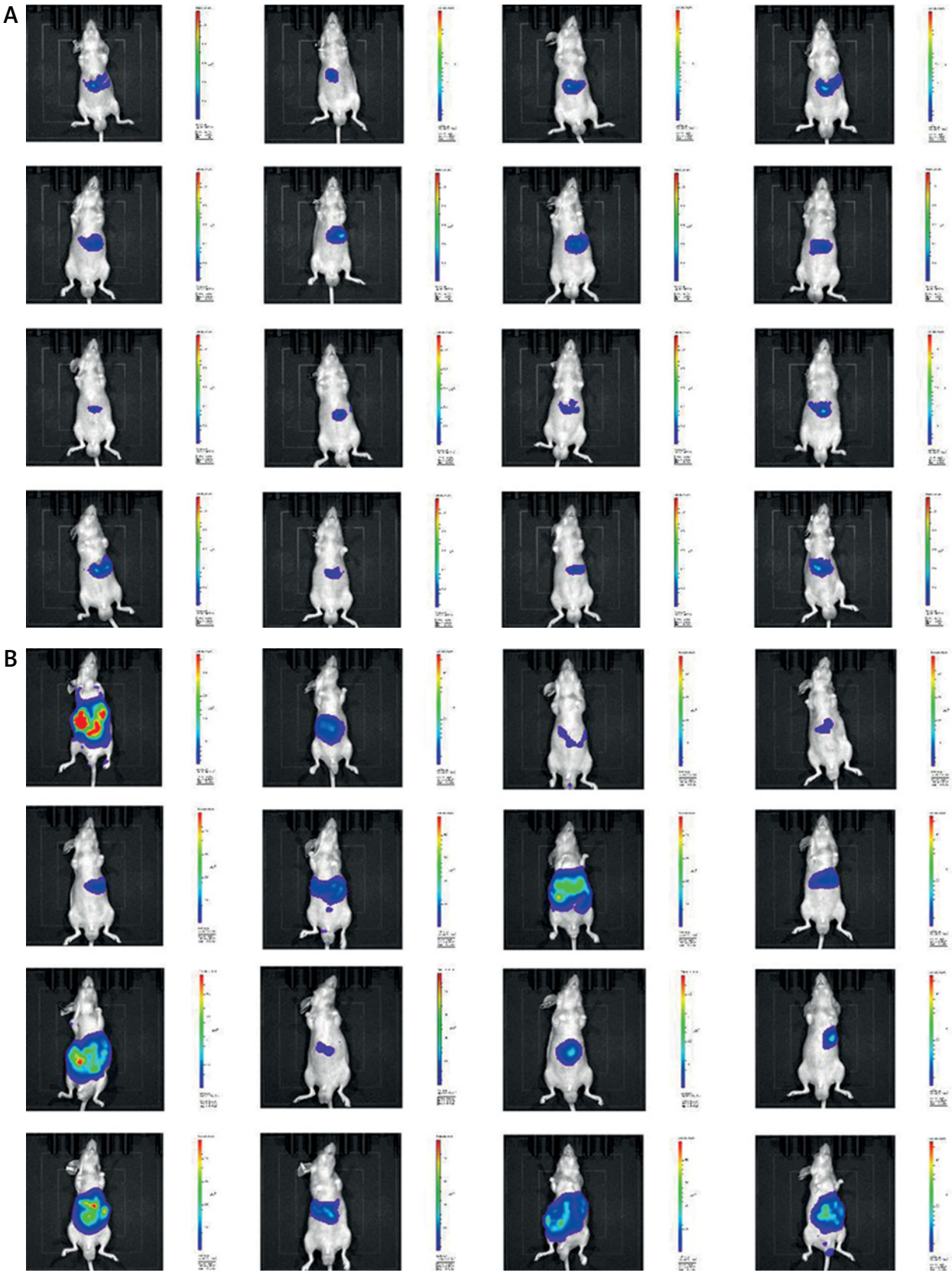

Figure 4. Longitudinal monitoring of orthotopic HCC progression. **A** – Baseline bioluminescence signal immediately after intrahepatic tumor implantation (day 0). **B** – Tumor progression monitored by *in vivo* imaging system at post-implantation day 7

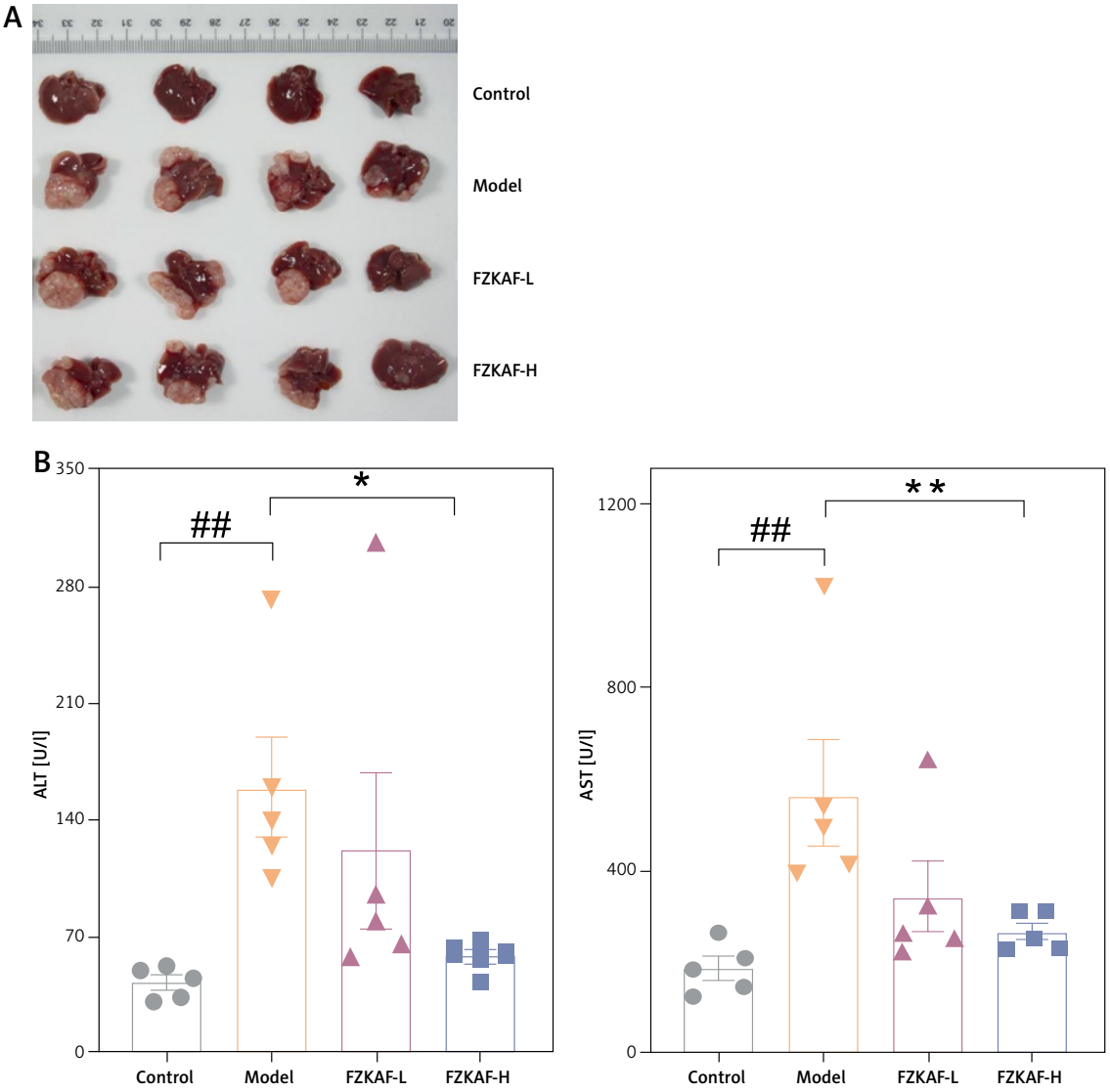

Figure 5. Anti-tumor activity of FZKAF in HCC. **A** – Effect of FZKAF on xenograft tumor growth from 97H cells. **B** – Impact of FZKAF on serum levels of liver function markers ALT and AST. *$p < 0.05$; ** or ##$p < 0.01$

mained within normal limits, but mitochondria displayed significant swelling and enlargement, with no notable RER dilation. Most notably, the FZKAF-H group (Figure 8 C) maintained near-normal cellular architecture, showing relatively intact perinuclear spaces, only minimal mitochondrial swelling, and completely preserved RER morphology. Autophagic activity showed no significant differences across all groups.

Effects of FZKAF on relevant signaling pathways

Integrated transcriptomic and proteomic analyses identified significantly differentially expressed proteins for molecular validation. Western blotting confirmed that FZKAF-containing serum modulated the expression levels of apoptosis-related proteins (BCL-2, BAX) as well as HIF-1α, KLF-4, and CA9 pro-

Table II. Impact of FZKAF on liver weight and tumor volume

Groups	Dosage [g/kg]	Liver weight [g]	Tumor volume [cm³]
Control	–	1.21 ±0.05	–
Model	–	2.75 ±1.75##	26.07 ±22.82
FZKAF-L	46.15	2.40 ±1.04	20.14 ±8.82
FZKAF-H	92.30	2.17 ±0.27**	17.07 ±17.07**

*##p < 0.01 compared to control group; **p < 0.01 compared to model group.*

Table III. Effects of FZKAF on body weight changes in tumor-bearing mice across treatment groups

Groups	Dosage [g/kg]	1 day	5 days	11 days	15 days	21 days	25 days
		Body weight [g]					
Control	–	22.49 ±1.62	22.42 ±1.14	24.26 ±0.87	24.24 ±1.07	23.35 ±4.37	25.80 ±1.07
Model	–	19.84 ±1.63	20.70 ±1.35	22.25 ±1.25	22.17 ±1.29	21.80 ±1.50	21.54 ±1.58
FZKAF-L	46.15	20.59 ±1.20	20.99 ±1.25	22.35 ±1.66	21.94 ±2.46	22.81 ±2.13	22.89 ±2.29
FZKAF-H	92.30	20.56 ±1.90	21.10 ±2.00	22.24 ±2.18	22.46 ±1.65	23.45 ±1.37	23.50 ±1.64*

*$P < 0.05$.

teins. Compared to the control group, both FZKAF-L and FZKAF-H groups exhibited significantly up-regulated KLF-4 protein expression ($p < 0.05$). Simultaneously, FZKAF-L and FZKAF-H groups showed down-regulated protein levels of BCL-2, BAX, HIF-1α, and CA9 ($p < 0.05$; Figure 9). These results collectively establish that FZKAF promotes tumor cell apoptosis and inhibits HCC cell proliferation.

Discussion

In our study, high-resolution liquid chromatography-mass spectrometry (LC-MS) analysis of blood-absorbed components identified 32 compounds derived from FZKAF, with nine potential anti-HCC constituents screened: albiflorin, eicosadienoic acid, catechin, coumarin, kaempferol, quercetin, arachidonic acid, equilin, and ergosterol peroxide. These bioactive components significantly inhibited 97H cell proliferation and induced apoptosis in both *in vitro* and *in vivo* HCC models. Concurrently, FZKAF substantially upregulated KLF4 protein expression and downregulated BCL-2, BAX, HIF-1α, and CA9 protein levels. These findings demonstrate that FZKAF, as a compound formula, likely exerts synergistic anti-HCC effects through multi-component, multi-target/pathway mechanisms, highlighting its therapeutic potential against liver cancer.

In recent years, substantial research has demonstrated that TCM formulas exhibit significant therapeutic effects against HCC, emerging as promising adjunctive therapeutic strategies for liver cancer treatment [8, 11, 12, 28–33]. For example, Kuan-Sin-Yin (KSY) decoction inhibited HCC cell mobility by downregulating C-C motif chemokine ligand 2 (CCL2), carcinoembryonic antigen-related cell adhesion molecule 1 (CEACAM1), and phosphoinositide-3-kinase regulatory subunit 3 (PIK3R3). However, KSY did not affect cell viability of HCC cells [28]. Shipi Xiaoji formula triggered ferroptosis in HCC cells, mediating its anti-tumor effects through the regulation of related genes and proteins [29]. Clinically, Fuzheng Jiedu Xiaoji (FZJX) combined with transarterial chemoembolization (TACE) significantly prolonged overall survival (OS) and progression-free survival (PFS) while reducing mortality in HCC patients. Mechanistically, FZJX suppressed proliferation and migration of liver cancer cells via modulating the AKT/cyclinD1/p21/p27 axis [12, 30]. By targeting the phosphoinositide 3-kinase/protein kinase B/mammalian target of rapamycin (PI3K/Akt/mTOR) pathway and boosting T-cell infiltration, Huqi formula suppressed HCC progression [31]. Da-Chai-Hu-Tang Formula impeded HepG2 cell progression and metastasis by modulating PI3K/AKT/STAT3-mediated cell cycle arrest and apoptosis [32]. Siwu decoction (SWD) suppressed myeloid-derived suppressor cells through tumor cell necroptosis induction, thereby inhibiting HCC [33]. Adjunctive Fuzheng Huayu treatment reduced HCC occurrence in entecavir-treated patients with chronic hepatitis B (CHB), potentially via its antifibrotic properties [8]. Entecavir combined with Biejia-Ruangan compound significantly reduced HCC risk and liver-related mortality in Chinese patients with CHB and advanced fibrosis or cirrhosis [11]. Collectively, the data establish that multi-herb formulations confer dual anti-HCC advantages, including direct suppression of oncogenesis and chemosensitization enhancement for molecularly targeted therapeutics.

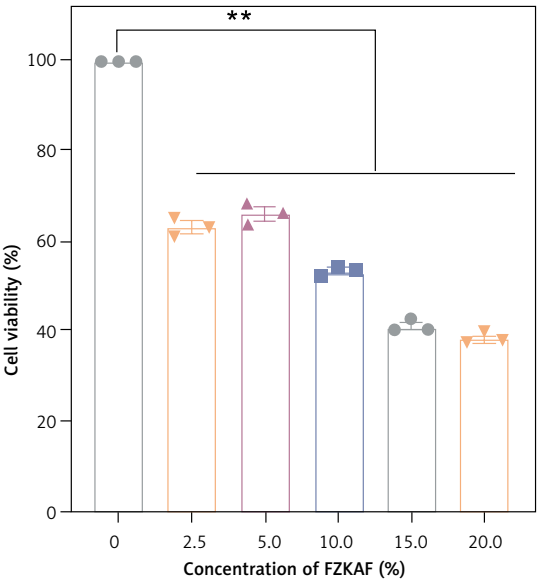

Figure 6. Effect of FZKAF on 97H cell proliferation. After 48 h of incubation with FZKAF-containing serum at concentrations of 0, 2.5, 5, 10, 15, and 20%, cell viability was measured with CCK-8. $^{**}p < 0.01$

LC-MS-guided bioactive compound screening coupled with mechanistic literature validation suggested albiflorin, kaempferol, and quercetin as primary mediators of FZKAF's anti-HCC pharmacological actions [33–35]. Albiflorin has been identified as a bioactive constituent of SWD, with demonstrated anti-HCC mechanisms consistent with those of the parent formula SWD [33]. Kaempferol derived from both persimmon leaves and *Alpinia officinarum* Hance targets hepatocellular carcinoma through distinct mechanisms: it sensitized cells to ABT-199-induced apoptosis via Mcl-1 inhibition and induced G2/M arrest by modulating the ATM/CHEK2/KNL1 pathway [34, 35]. Extensive studies confirm quercetin's significant anti-HCC efficacy [36–38]. Through multi-target synergistic mechanisms, this flavonoid suppresses HCC progression by directly binding to checkpoint kinase 1 (CHK1), a hub regulator of DNA damage response – forming stable complexes, downregulating prolyl 4-hydroxylase subunit alpha 2 (P4HA2), the rate-limiting enzyme in collagen biosynthesis, and dual-pathway blockade targeting both the PI3K/Akt/mTOR pro-survival axis and the interleukin-6/

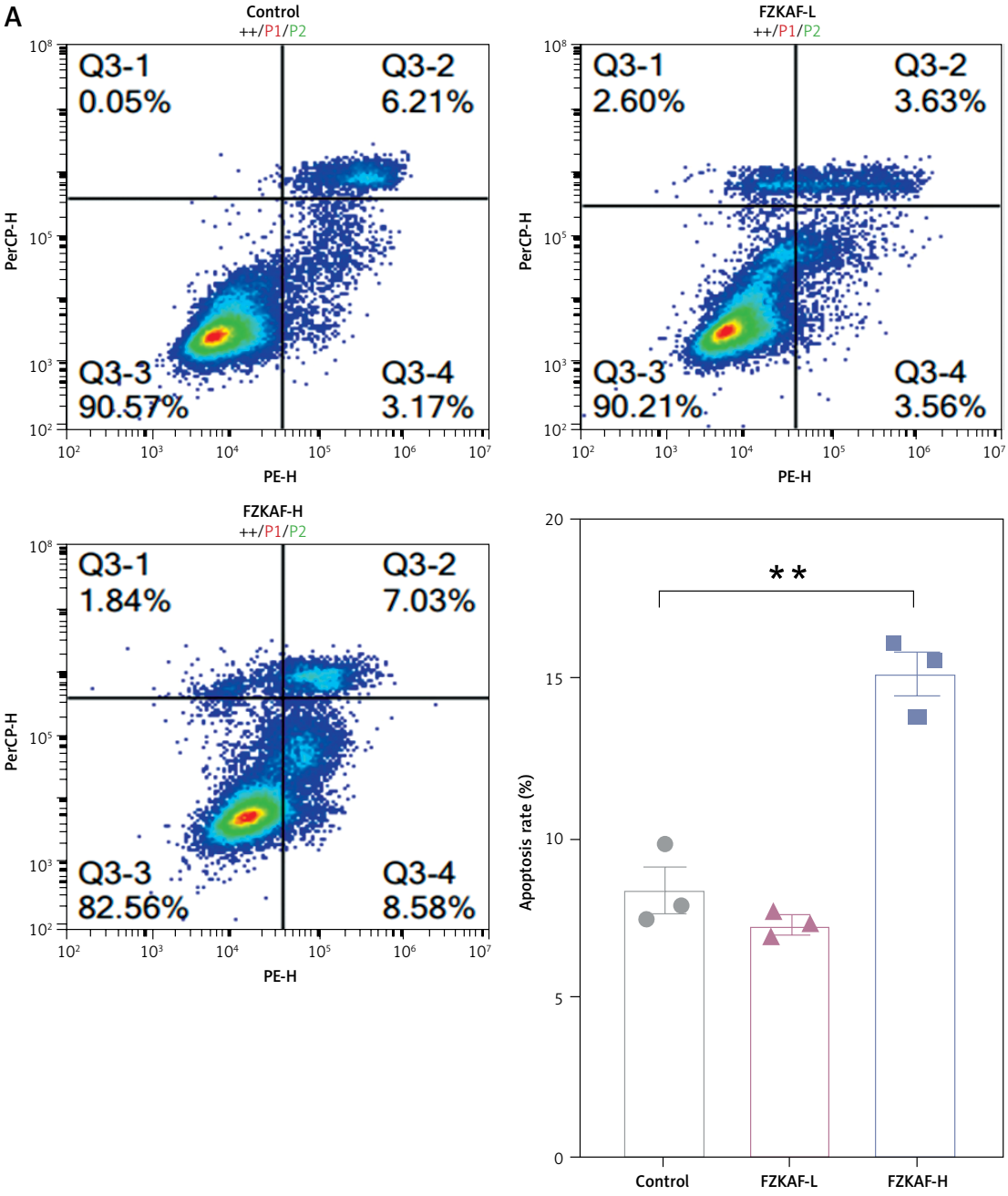

Figure 7. Effect of FZKAF on 97H cell apoptosis and cell cycle arrest. **A** – Cell apoptosis with Annexin V-FITC/PI double staining. *$p < 0.05$; **$p < 0.01$

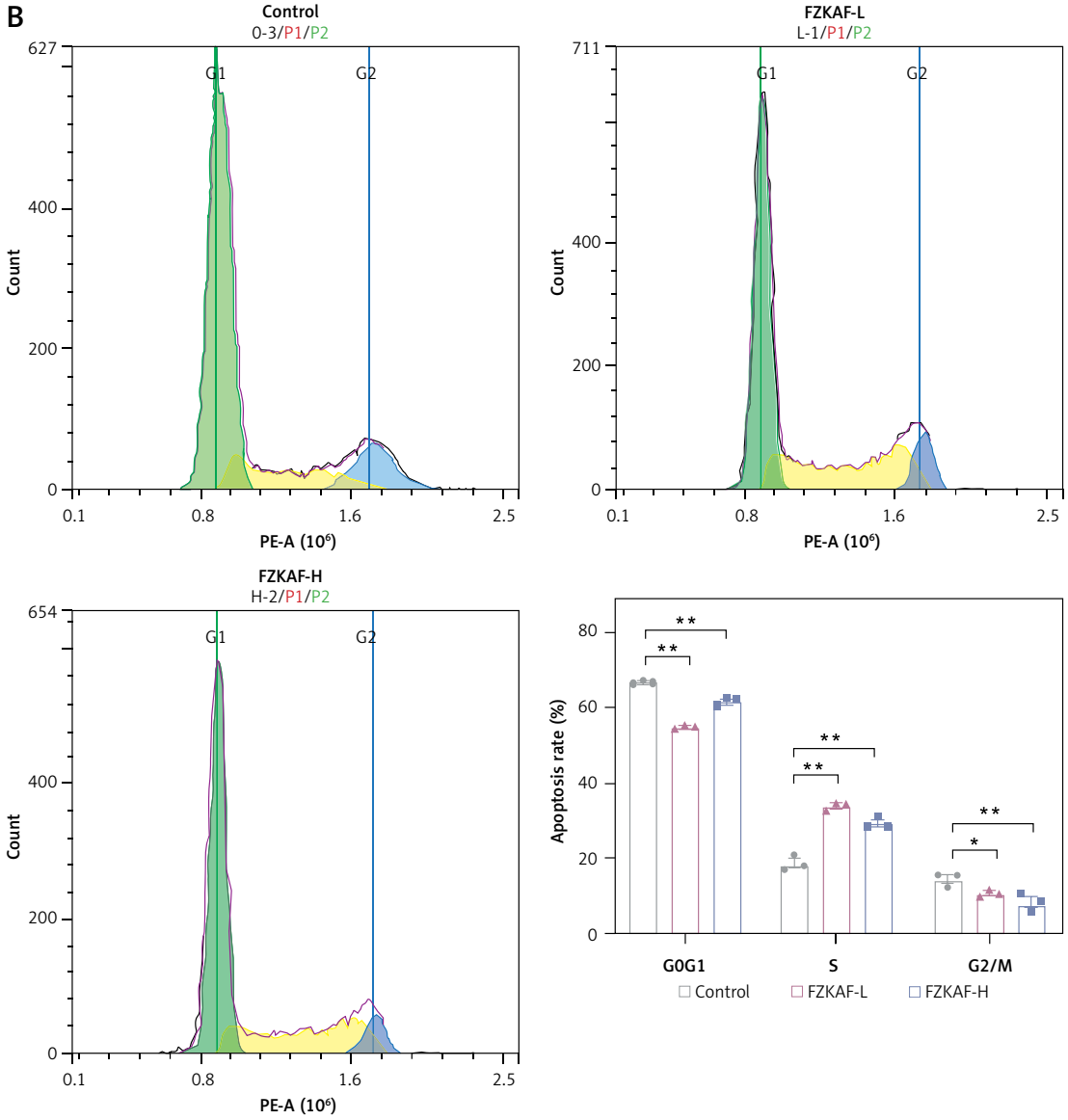

Figure 7. Cont. **B** – Cell cycle arrest with PI staining. *$p < 0.05$; **$p < 0.01$

mitogen-activated protein kinase kinase/extracellular signal-regulated kinase (IL6/MEK/ERK) inflammatory-metabolic cascade [36–38]. These actions collectively induce caspase-dependent apoptosis at the molecular level while inhibiting proliferation, migration, and epithelial-mesenchymal transition (EMT) at the cellular level. Crucially, under hyperglycemic conditions, quercetin significantly reverses malignant phenotypes in diabetes-associated HCC through suppression of the IL6-Janus kinase/signal transducer and activator of transcription 3 (JAK/STAT3) signaling axis [36–38].

Quercetin activates KLF4 expression via the nuclear factor erythroid 2-related factor 2 (Nrf2)/antioxidant response element (ARE) pathway [39, 40] while suppressing HIF-1α stability through PI3K/AKT/mTOR inhibition [41]. Kaempferol synergistically enhances mitochondrial apoptosis via the reactive oxygen species (ROS)/c-Jun N-terminal kinase (JNK) cascade [42], collectively elevating the pro-apoptotic BCL2-associated X protein (Bax)/B-cell lymphoma 2 (Bcl-2) ratio with quercetin [43]. Complementary mechanisms include: albiflorin potentially counteracting CA9-mediated microenvironment acidification by modulating tryptophan metabolism; catechin upregulating KLF4 to inhibit tumor proliferation [44]; ergosterol peroxide inducing cancer cell death via Bax activation and Forkhead box protein O3 (FoxO3)-mediated apoptosis signaling [45], and coumarin binding HIF-1α to promote its degradation, thereby impairing glycolysis and promoting apoptosis [46]. These results indicate that FZKAF may modulate the progression of HCC through multi-mechanism and multi-target regulation. Crucially, both

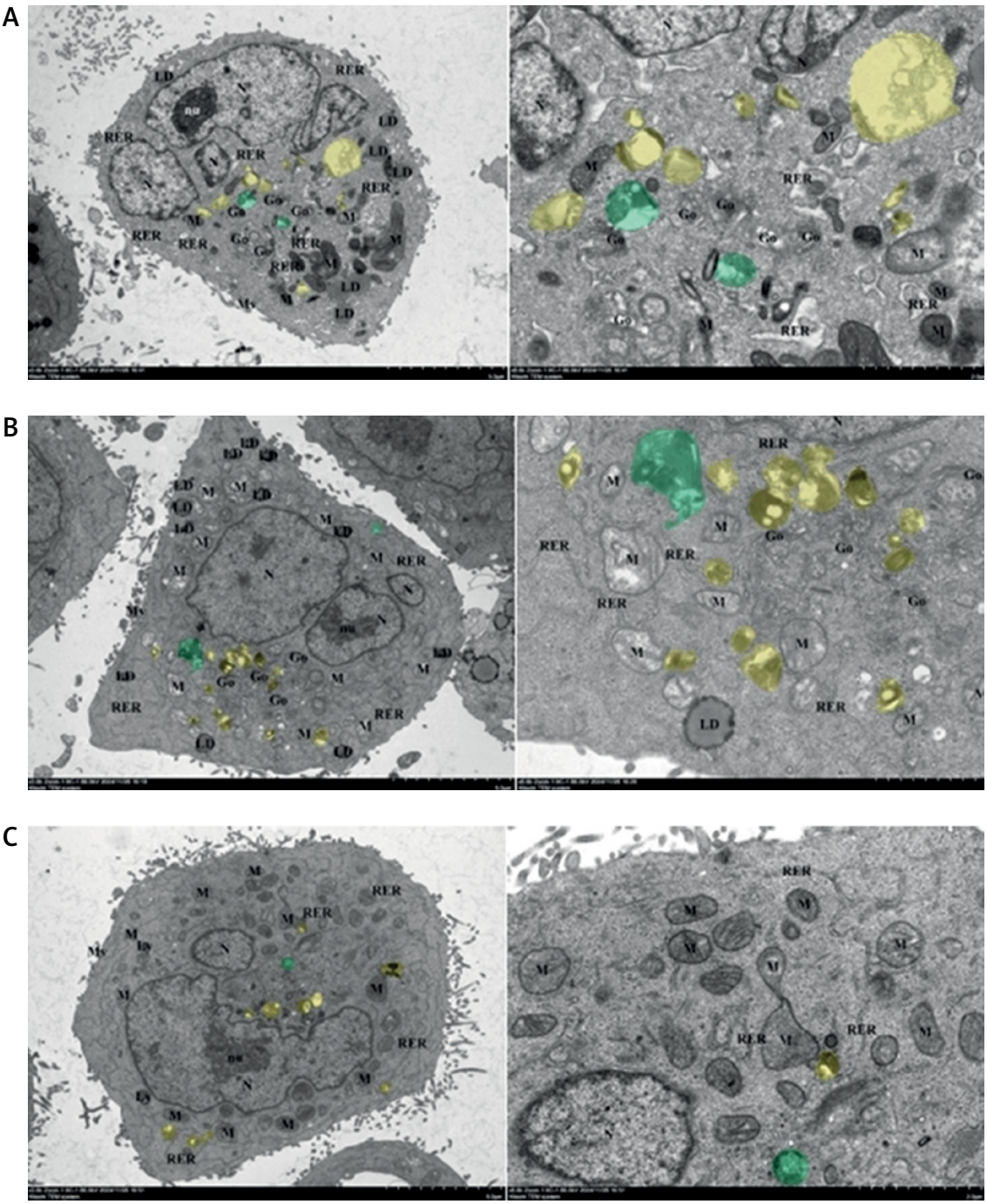

Figure 8. Effects of FZKAF on cell morphology. TEM analysis revealed distinct morphological alterations among the three treatment groups following exposure to control group (**A**), 10% FZKAF-containing serum (**B**), and 20% FZKAF-containing serum (**C**)

KLF4 and HIF-1α function as upstream modulators of CA9 [47–49], suggesting concurrent CA9 suppression. CA9, a transmembrane glycoprotein transcriptionally regulated by HIF-1α, is predominantly expressed under hypoxic conditions. It modulates intracellular and extracellular pH through catalytic hydration of carbon dioxide. This pH-regulating function is critical for maintaining tumor microenvironment stability and promoting cancer progression by facilitating tumor growth, invasion, and metastasis [50]. As a carbonic anhydrase inhibitor, acetazolamide offers a novel therapeutic approach for experimentally induced HCC. It modulates hepatic biomarkers, antioxidant status, inflammatory markers, and autophagy through downregulation of CA9 gene expression [51]. CA9 also acts as a downstream target facilitating the tumor-promoting actions of DDX11-

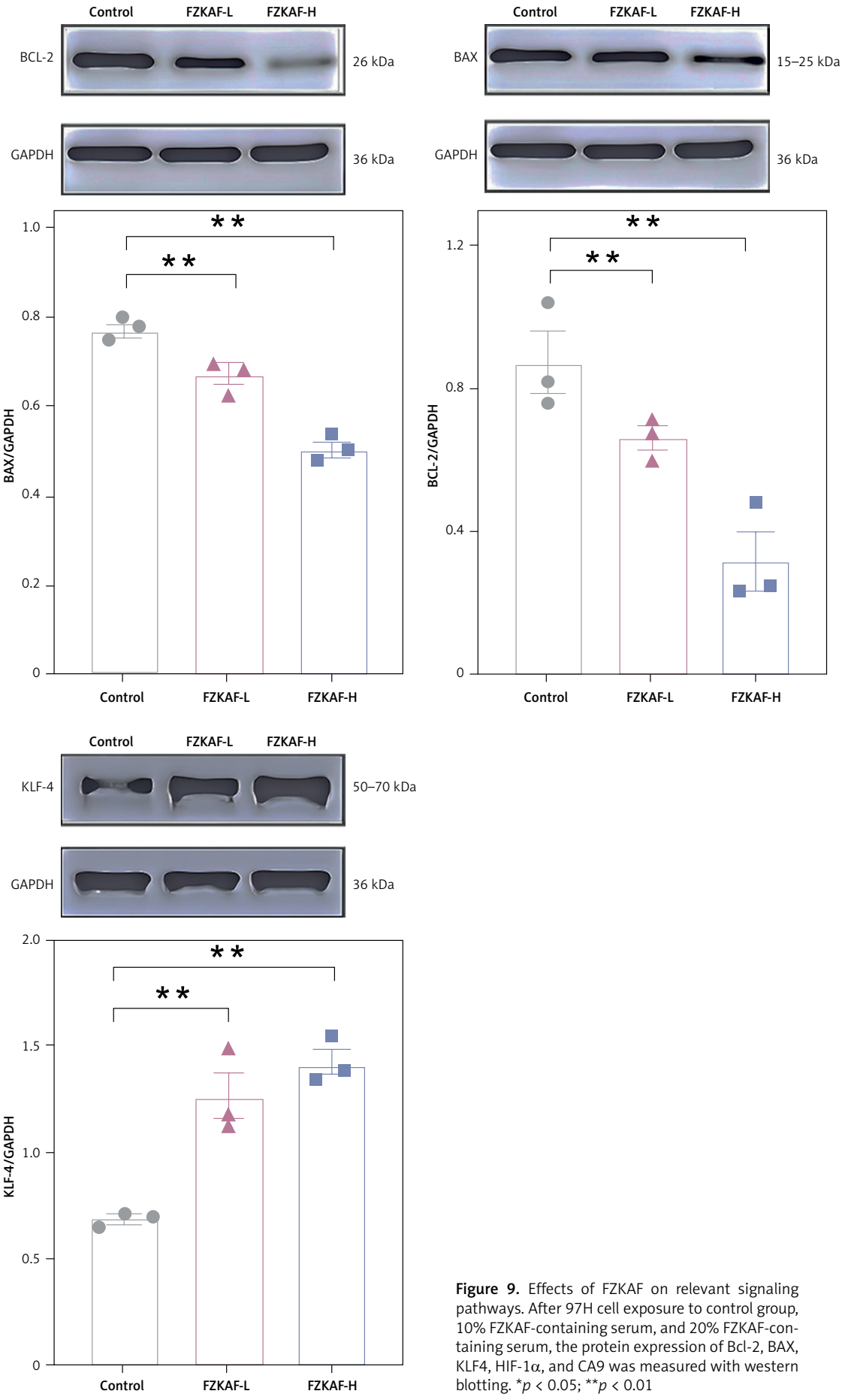

Figure 9. Effects of FZKAF on relevant signaling pathways. After 97H cell exposure to control group, 10% FZKAF-containing serum, and 20% FZKAF-containing serum, the protein expression of Bcl-2, BAX, KLF4, HIF-1α, and CA9 was measured with western blotting. *$p < 0.05$; **$p < 0.01$

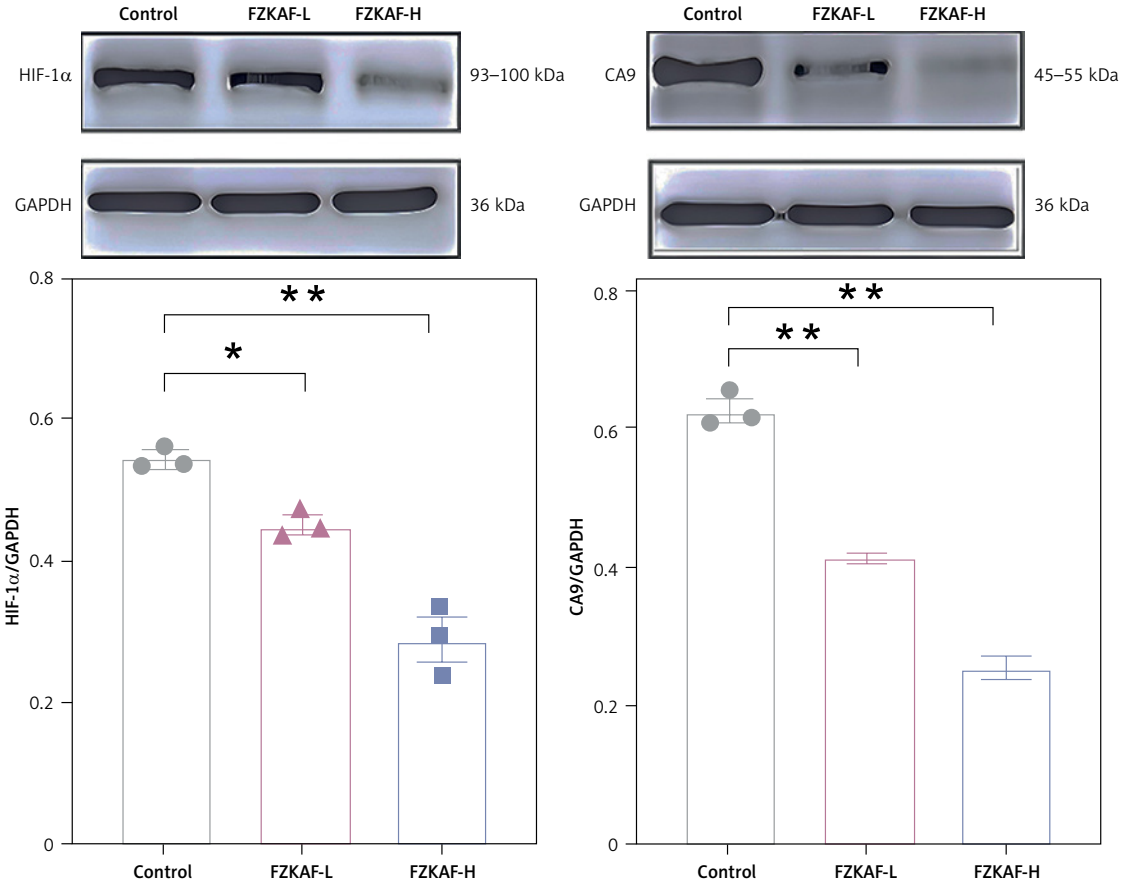

Figure 9. Cont. *$p < 0.05$; **$p < 0.01$

AS1 in HCC [52]. Wei *et al.* [53] established that sorafenib-mediated metallothionein 1 G (MT1G) activation drives KLF4-dependent HIF1A suppression, resulting in transcriptional inhibition of CA9 in HCC. Our data validate these literature findings that FZKAF treatment significantly increased KLF4 protein expression while synchronously downregulating HIF-1α and CA9 protein expression in HCC. The data establish that FZKAF targets the KLF4/HIF-1α/CA9 axis to alleviate intratumoral hypoxia, thereby suppressing hepatocarcinogenesis.

Owing to the multi-component nature of TCM formulae and their polypharmacology in tumor regulation, this study has inherent limitations. First, we only partially elucidated select potential targets, without comprehensive mechanistic exploration. Second, the *in vitro* experiments employed medicated serum administration, which may introduce non-specific interference from unidentified serum components to 97H cells. Third, functional validation through KLF4 knockout and overexpression studies, essential for confirming the regulatory role of the KLF4/HIF-1α/CA9 axis in HCC, was not performed.

In conclusion, integrated *in vitro* and *in vivo* models demonstrate FZKAF's potent anti-HCC efficacy through suppression of proliferation and migration, and induction of apoptosis. Mechanistically, FZKAF may target the KLF4/HIF-1α/CA9 axis to inhibit HCC progression. While showing promise as an adjunctive HCC therapy, clinical translation requires systematic pharmacodynamic characterization and therapeutic optimization.

Acknowledgments

Yi Cui and Yuhan Zhang contributed equally to this work.

Funding

This study was supported by the Science and Technology Talent Program for Young and Middle-aged Scholars, Administration of Traditional Chinese Medicine of Shaanxi Province (2023-ZQNY-016); Clinical Collaboration and Innovation Program for Integrated Traditional Chinese and Western Medicine, Administration of Traditional Chinese Medicine of Shaanxi Province (2020-ZXY-008).

Ethical approval

This animal experiment was approved by the Animal Ethics Committee of Xi'an Jiaotong University (approval number: 2023-20).

Conflict of interest

The authors declare no conflict of interest.

References

1. Bray F, Laversanne M, Sung H, et al. Global cancer statistics 2022: GLOBOCAN estimates of incidence and mortality worldwide for 36 cancers in 185 countries. CA Cancer J Clin 2024; 74: 229-63.
2. Han B, Zheng R, Zeng H, et al. Cancer incidence and mortality in China, 2022. J Natl Cancer Cent 2024; 4: 47-53.
3. Devarbhavi H, Asrani SK, Arab JP, Nartey YA, Pose E, Kamath PS. Global burden of liver disease: 2023 update. J Hepatol 2023; 79: 516-37.
4. Pazgan-Simon M, Szymanek-Pasternal A, Górka-Dynysiewicz J, et al. Serum chemerin level in patients with liver cirrhosis and primary and multifocal hepatocellular carcinoma with consideration of insulin level. Arch Med Sci 2024; 20: 1504-10.
5. Wei L, Wang Z, Jing N, et al. Frontier progress of the combination of modern medicine and traditional Chinese medicine in the treatment of hepatocellular carcinoma. Chin Med 2022; 17: 90.
6. Xu L, Wang S, Zhuang L, et al. Jian Pi Li Qi Decoction alleviated postembolization syndrome following transcatheter arterial chemoembolization for hepatocellular carcinoma: a randomized, double-blind, placebo-controlled trial. Integr Cancer Ther 2016; 15: 349-57.
7. Peng Y, Wu X, Zhang Y, et al. An overview of traditional chinese medicine in the treatment after radical resection of hepatocellular carcinoma. J Hepatocell Carcinoma 2023; 10: 2305-21.
8. Fan H, Lei S, Zhao Z, et al. Beneficial effects of traditional Chinese medicine fuzheng huayu on the occurrence of hepatocellular carcinoma in patients with compensated chronic hepatitis B cirrhosis receiving entecavir: a multicenter retrospective cohort study. J Clin Transl Hepatol 2024; 12: 505-15.
9. Lin J, Guo H, Qin H, Zhang X, Sheng J. Integration of meta-analysis and network pharmacology analysis to investigate the pharmacological mechanisms of traditional Chinese medicine in the treatment of hepatocellular carcinoma. Front Pharmacol 2024; 15: 1374988.
10. Luo J, Zhang H, Jiang D, Li Y, Ye T. Uncovering the role of RPL8 in glutathione synthesis-dependent ferroptosis control in hepatocellular carcinoma. Arch Med Sci 2025; 21: 1513-35.
11. Ji D, Chen Y, Bi J, et al. Entecavir plus Biejia-Ruangan compound reduces the risk of hepatocellular carcinoma in Chinese patients with chronic hepatitis B. J Hepatol 2022; 77: 1515-24.
12. Yang X, Feng Y, Liu Y, et al. Fuzheng Jiedu Xiaoji formulation inhibits hepatocellular carcinoma progression in patients by targeting the AKT/CyclinD1/p21/p27 pathway. Phytomedicine 2021; 87: 153575.
13. Cao J, Huang J, Gui S, Chu X. Preparation, synergism, and biocompatibility of in situ liquid crystals loaded with sinomenine and 5-fluorouracil for treatment of liver cancer. Int J Nanomedicine 2021; 16: 3725-39.
14. Luo Y, Lin W, Xiang S, et al. Paeoniflorin inhibits chronic restraint stress-induced progression of hepatocellular carcinoma through suppressing norepinephrine-induced activation of hepatic stellate cells via SRC/AKT/ERK pathways. J Ethnopharmacol 2025; 344: 119517.
15. Jinhua LI, Chunping L, Yueyang Z, et al. Fuzheng Kang' ai decoction inhibits cell proliferation, migration and invasion by modulating mir-21-5p/human phosphatase and tensin homology deleted on chromosome ten in lung cancer cells. J Tradit Chin Med 2022; 42: 344-52.
16. Yang XB, Wu WY, Long SQ, Deng H, Pan ZQ. Effect of gefitinib plus Chinese herbal medicine (CHM) in patients with advanced non-small-cell lung cancer: a retrospective case-control study. Complement Ther Med 2014; 22: 1010-8.
17. Wang S, Peng Z, Li W, Long S, Xiao S, Wu W. Fuzheng Kang-Ai decoction enhances the effect of Gefitinib-induced cell apoptosis in lung cancer through mitochondrial pathway. Cancer Cell Int 2020; 20: 185.
18. Li L, Wang S, Zheng F, Wu W, Hann SS. Chinese herbal medicine Fuzheng Kang-Ai decoction sensitized the effect of gefitinib on inhibition of human lung cancer cells through inactivating PI3-K/Akt -mediated suppressing MUC1 expression. J Ethnopharmacol 2016; 194: 918-29.
19. Zheng F, Zhao Y, Li X, et al. The repression and reciprocal interaction of DNA methyltransferase 1 and specificity protein 1 contributes to the inhibition of MET expression by the combination of Chinese herbal medicine FZKA decoction and erlotinib. J Ethnopharmacol 2019; 239: 111928.
20. Tang Q, Xu M, Long S, et al. FZKA reverses gefitinib resistance by regulating EZH2/Snail/EGFR signaling pathway in lung adenocarcinoma. J Ethnopharmacol 2024; 318: 116646.
21. Yang Y, Jiang B, Shi L, et al. The potential of natural herbal plants in the treatment and prevention of non-small cell lung cancer: an encounter between ferroptosis and mitophagy. J Ethnopharmacol 2025; 346: 119555.
22. Zhao YY, Yang YQ, Sheng HH, et al. GPX4 Plays a crucial role in fuzheng kang'ai decoction-induced non-small cell lung cancer cell ferroptosis. Front Pharmacol 2022; 13: 851680.
23. Huang J, Shi R, Chen F, et al. Exploring the anti-hepatocellular carcinoma effects of Xianglian Pill: integrating network pharmacology and RNA sequencing via in silico and in vitro studies. Phytomedicine 2024; 133: 155905.
24. Xie YQ, Yan FN, Yu LH, Yan HW, Kong YX, Yang ZY. Mechanism of Shashen-Maidong herb pair in treating hepatocellular carcinoma using network pharmacology and experimental validation. J Ethnopharmacol 2025; 337: 118954.
25. Qin MY, Huang SQ, Zou XQ, et al. Drug-containing serum of rhubarb-astragalus capsule inhibits the epithelial-mesenchymal transformation of HK-2 by downregulating TGF-β1/p38MAPK/Smad2/3 pathway. J Ethnopharmacol 2021; 280: 114414.
26. Shi Y, Liu Q, Chen W, et al. Protection of Taohong Siwu Decoction on PC12 cells injured by oxygen glucose deprivation/reperfusion via mitophagy-NLRP3 inflammasome pathway in vitro. J Ethnopharmacol 2023; 301: 115784.
27. Percie du Sert N, Hurst V, Ahluwalia A, et al. The ARRIVE guidelines 2.0: updated guidelines for reporting animal research. J Cereb Blood Flow Metab 2020; 40: 1769-77.
28. Chen CT, Chen CF, Lin TY, et al. Traditional Chinese medicine Kuan-Sin-Yin decoction inhibits cell mobility via

downregulation of CCL2, CEACAM1 and PIK3R3 in hepatocellular carcinoma cells. J Ethnopharmacol 2023; 317: 116834.
29. Yang R, Fu X, Wang Z, et al. Unlocking the potential of Traditional Chinese Medicine (TCM): Shipi Xiaoji formula (SPXJF) as a novel ferroptosis inducer in hepatocellular carcinoma. J Ethnopharmacol 2025; 340: 119236.
30. Zhang Y, Shi K, Li YQ, Liu Y, Feng Y, Wang XB. Efficacy and safety of Fuzheng Jiedu Xiaoji formula combined with conventional western therapy in advanced HBV-HCC: a single-center, randomized controlled trial. Chin J Integr Med 2025; 31: 867-76.
31. Yin D, Li X, Yang X, et al. Huqi formula suppresses hepatocellular carcinoma growth by modulating the PI3K/AKT/mTOR pathway and promoting T cell infiltration. Chin Med 2025; 20: 25.
32. Duan ZW, Liu Y, Zhang PP, et al. Da-Chai-Hu-Tang formula inhibits the progression and metastasis in HepG2 cells through modulation of the PI3K/AKT/STAT3-induced cell cycle arrest and apoptosis. J Ethnopharmacol 2024; 331: 118293.
33. Feng Z, Chan YT, Lu Y, et al. Siwu decoction suppress myeloid-derived suppressor cells through tumour cells necroptosis to inhibit hepatocellular carcinoma. Phytomedicine 2024; 133: 155913.
34. Chen L, Jiang XD, Liu XP, et al. Mcl-1 is an important target protein for kaempferol from persimmon leaves in sensitizing ABT-199 to induce apoptosis in hepatoma cancer cells. Med Oncol 2025; 42: 146.
35. Li X, Zhou M, Zhu Z, et al. Kaempferol from Alpinia officinarum hance induces G2/M cell cycle arrest in hepatocellular carcinoma cells by regulating the ATM/CHEK2/KNL1 pathway. J Ethnopharmacol 2024; 333: 118430.
36. Lin F, Zhou W, Yuan X, Liu S, He Z. Mechanistic study of quercetin in the treatment of hepatocellular carcinoma with diabetes via MEK/ERK pathway. Int Immunopharmacol 2024; 142: 113194.
37. Chen F. Inhibiting Pink1/Parkin-mediated mitophagy enhances the anticancer effects of quercetin in hepatocellular carcinomaf. Biochem Biophys Res Commun 2024; 712-713: 149899.
38. Chen W, Li Y, Zhang C, et al. Multi-omics and experimental validation reveal anti-HCC mechanisms of Tibetan Liuwei Muxiang Pill and Quercetin. Pharmaceuticals (Basel) 2025; 18: 900.
39. Tanigawa S, Fujii M, Hou DX. Action of Nrf2 and Keap1 in ARE-mediated NQO1 expression by quercetin. Free Radic Biol Med 2007; 42: 1690-703.
40. Wang Z, Bi Z, Bamrah J, et al. Nrf2 drives epigenetic reprogramming and acts as the master regulator of KLF4 expression and activity in arsenic-induced transformation. Adv Sci (Weinh) 2025; 12: e00221.
41. Zalpoor H, Bakhtiyari M, Liaghat M, Nabi-Afjadi M, Ganjalikhani-Hakemi M. Quercetin potential effects against SARS-CoV-2 infection and COVID-19-associated cancer progression by inhibiting mTOR and hypoxia-inducible factor-1α (HIF-1α). Phytother Res 2022; 36: 2679-82.
42. Park SJ, Kim DW, Lim SR, et al. Kaempferol blocks the skin fibroblastic interleukin 1β expression and cytotoxicity induced by 12-O-tetradecanoylphorbol-13-acetate by suppressing c-Jun N-terminal kinase. Nutrients 2021; 13: 3079.
43. Hamid Reza Ghaderi J, Sedigheh S, Abbas Zakeri B. Flavonoids kaempferol (KAE) and quercetine (QUE) inhibited proliferation of human leukemia THP-1 cells by up regulation of pro-apoptotic protein Bax and caspase 3/8 expression and down regulation of anti-apoptotic proteins Bcl-2, Bcl-xl and Mcl-1 expression. Ann Cancer Res Ther 2021; 29: 41-6.
44. Ma Y, Shi Y, Li W, Sun A, Zang P, Zhang P. Epigallocatechin-3-gallate regulates the expression of Kruppel-like factor 4 through myocyte enhancer factor 2A. Cell Stress Chaperones 2014; 19: 217-26.
45. Li X, Wu Q, Bu M, et al. Ergosterol peroxide activates Foxo3-mediated cell death signaling by inhibiting AKT and c-Myc in human hepatocellular carcinoma cells. Oncotarget 2016; 7: 33948-59.
46. Almatroodi SA, Almatroudi A, Alhumaydhi FA, Alsahli MA, Rahmani AH, Khan AA. Potential therapeutic targets of epigallocatechin gallate (EGCG), the most abundant catechin in green tea, and its role in the therapy of various types of cancer. Molecules 2020; 25: 3146.
47. Nan Y, Wu X, Luo Q, et al. OTUB2 silencing promotes ovarian cancer via mitochondrial metabolic reprogramming and can be synthetically targeted by CA9 inhibition. Proc Natl Acad Sci USA 2024; 121: e2315348121.
48. White B, Wang Z, Dean M, et al. Acidosis attenuates the hypoxic stabilization of HIF-1α by activating lysosomal degradation. J Cell Biol 2025; 224: e202409103.
49. Muniyandi A, Hartman GD, Sishtla K, et al. Ref-1 is overexpressed in neovascular eye disease and targetable with a novel inhibitor. Angiogenesis 2025; 28: 11.
50. Ronca R, Supuran CT. Carbonic anhydrase IX: an atypical target for innovative therapies in cancer. Biochim Biophys Acta Rev Cancer 2024; 1879: 189120.
51. Tamim YM, Soliman ML, Sayed MM, et al. Acetazolamide suppresses the progression of hepatocellular carcinoma induced by diethylnitrosamine in Wistar albino rats. Fundam Clin Pharmacol 2024; 38: 1045-58.
52. Li Y, Shi M, Bie B, et al. NRF1-induced lncRNA DDX11-AS1 contributes to the progression of hepatocellular carcinoma via activating CA9 expression and the MEK/ERK pathway. J Hepatocell Carcinoma 2025; 12: 891-908.
53. Wei T, Lin R, Fu X, et al. Epigenetic regulation of the DNMT1/MT1G/KLF4/CA9 axis synergises the anticancer effects of sorafenib in hepatocellular carcinoma. Pharmacol Res 2022; 180: 106244.